

Supporting information

**Tailored design of ruthenium molecular catalysts with 2, 2'-bipyridine-6, 6'-dicarboxylate and pyrazole based ligand for water oxidation**

Quentin Daniel<sup>a</sup>, Lei Wang<sup>a</sup>, Lele Duan<sup>a</sup>, Fusheng Li<sup>a</sup> and Licheng Sun<sup>ab\*</sup>

<sup>a</sup>*Department of Chemistry, KTH Royal Institute of Technology, 10044 Stockholm, Sweden.*

<sup>b</sup>*State Key Laboratory of Fine Chemicals, DUT-KTH Joint Education and Research Center on Molecular Devices, Dalian University of Technology (DUT), Dalian 116024, P. R. China.*

CONTENTS

<sup>1</sup> H-NMR study .....	2
O <sub>2</sub> detection .....	8
Differential pulse voltammetry .....	11

# $^1\text{H}$ -NMR STUDY

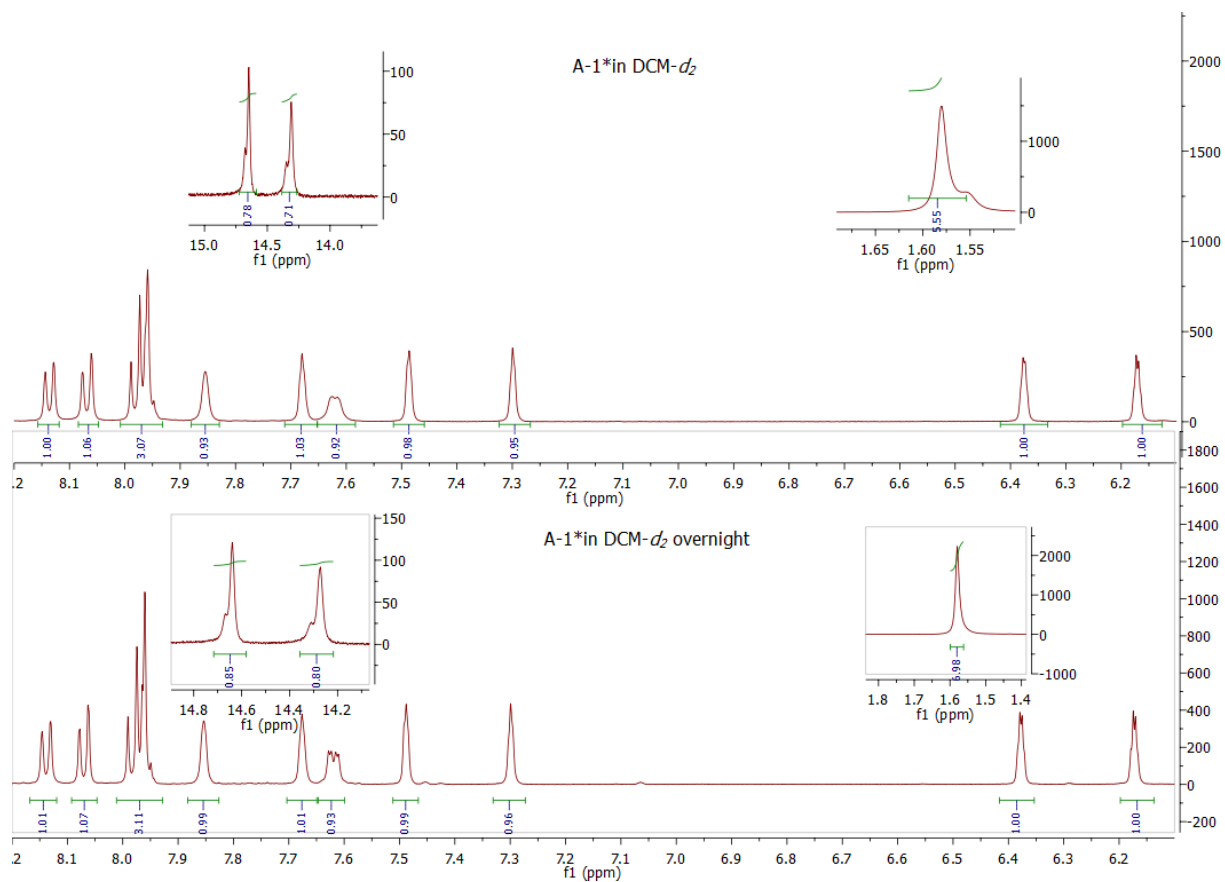


Figure S1.  $^1\text{H}$  NMR of **A-1\*** in dichloromethane- $d_2$  (DCM- $d_2$ ).

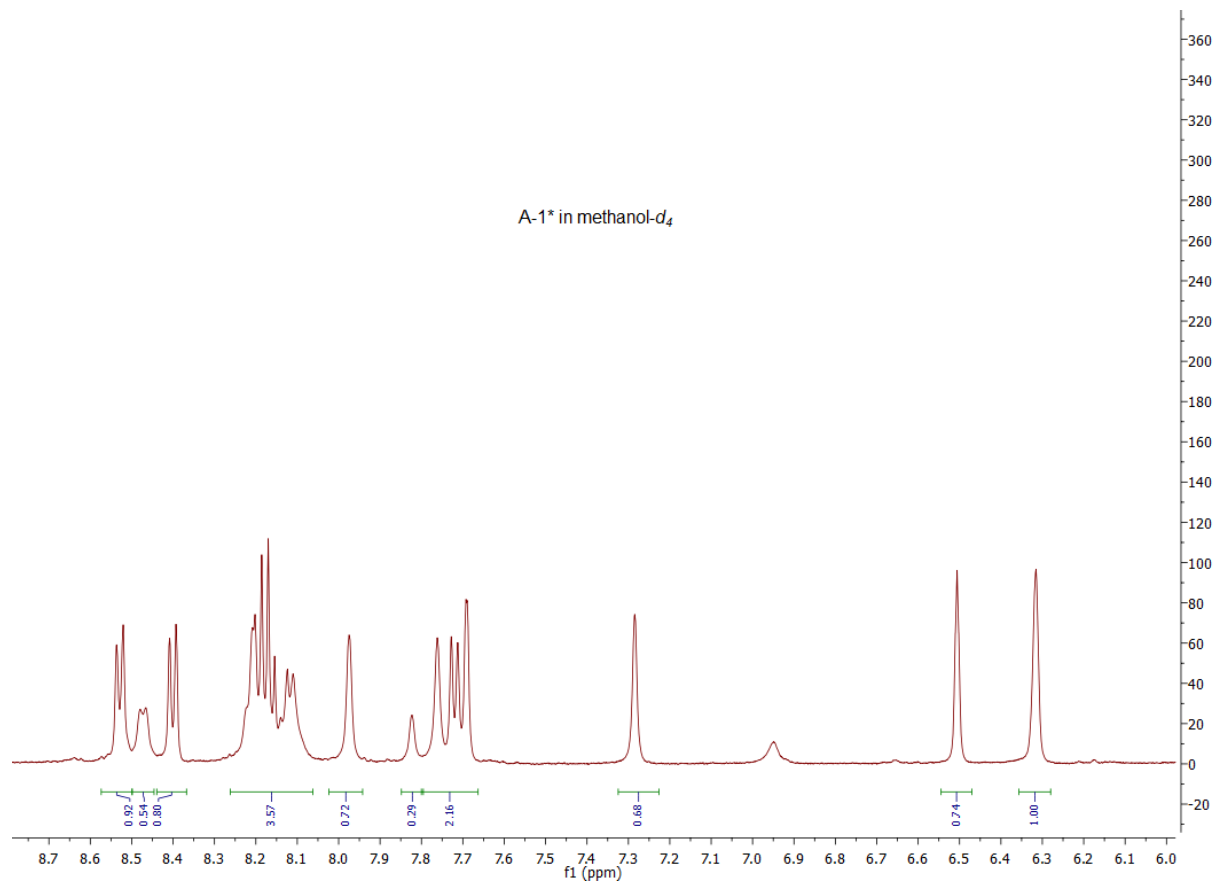


Figure S2.  $^1\text{H}$  NMR of A-1\* in methanol- $d_4$ .

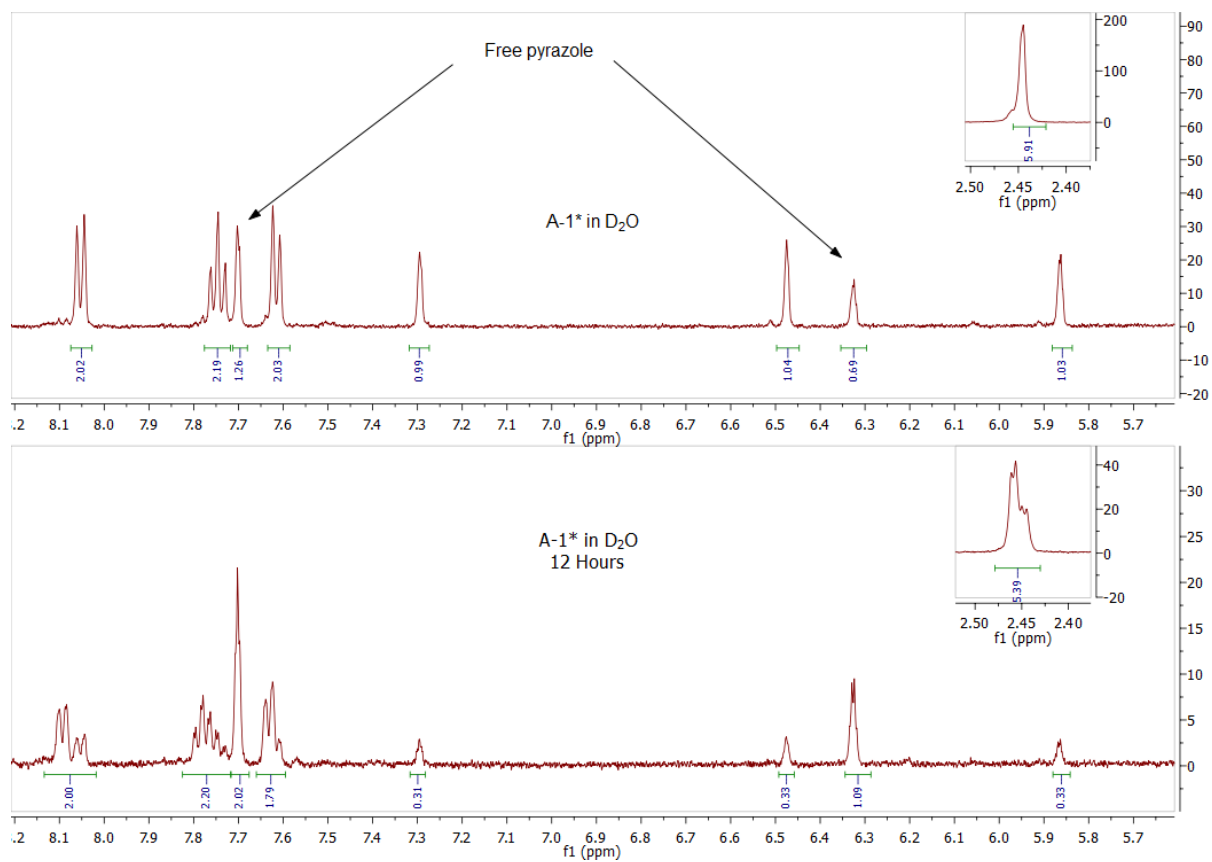


Figure S3. Stability test of **A-1\*** in D<sub>2</sub>O solution.

The loss of the equatorial ligand occurs in time scale of seconds while the loss of the axial pyrazole occurs an hour time scale.

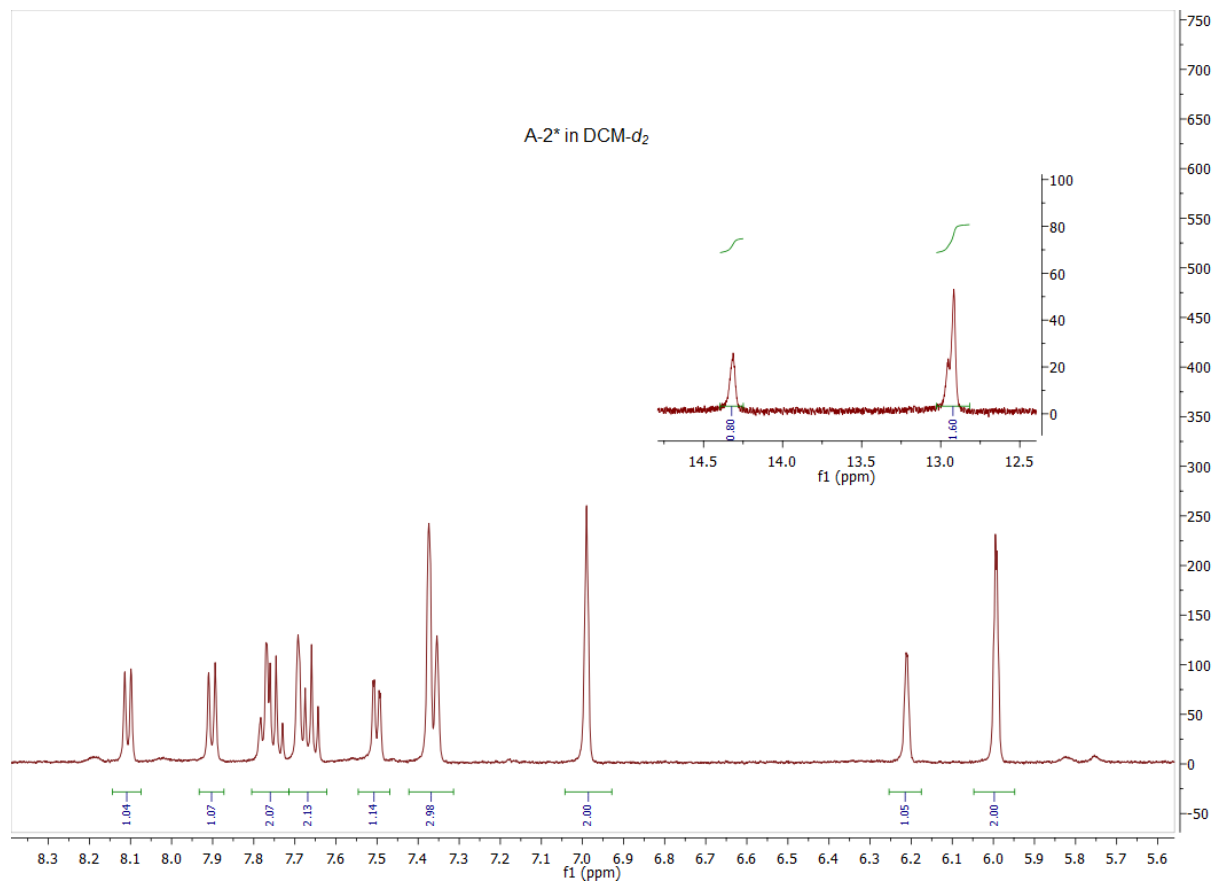


Figure S4.  $^1\text{H}$  NMR of A-2\* in dichloromethane- $d_2$  (DCM- $d_2$ ).

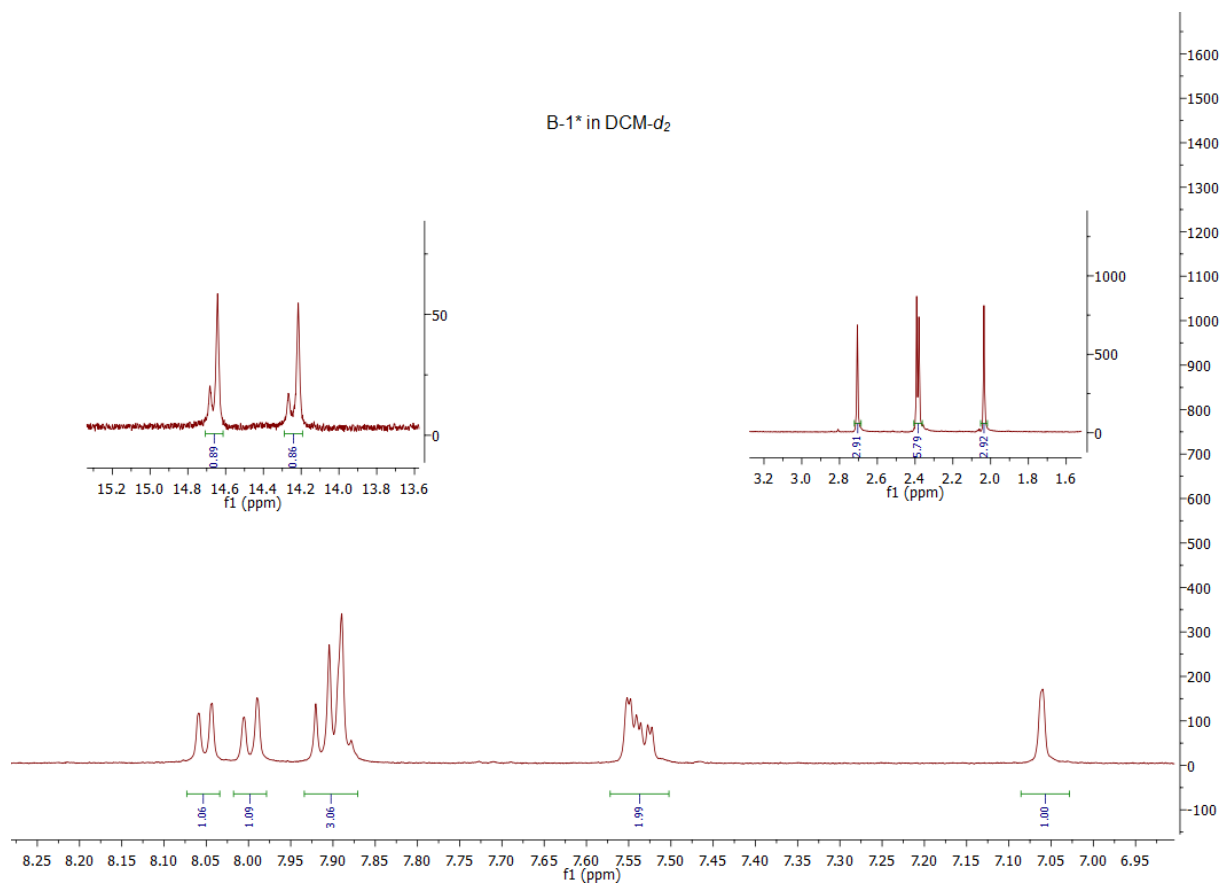


Figure S5.  $^1\text{H}$  NMR of **B-1\*** in dichloromethane- $d_2$  (DCM- $d_2$ ).

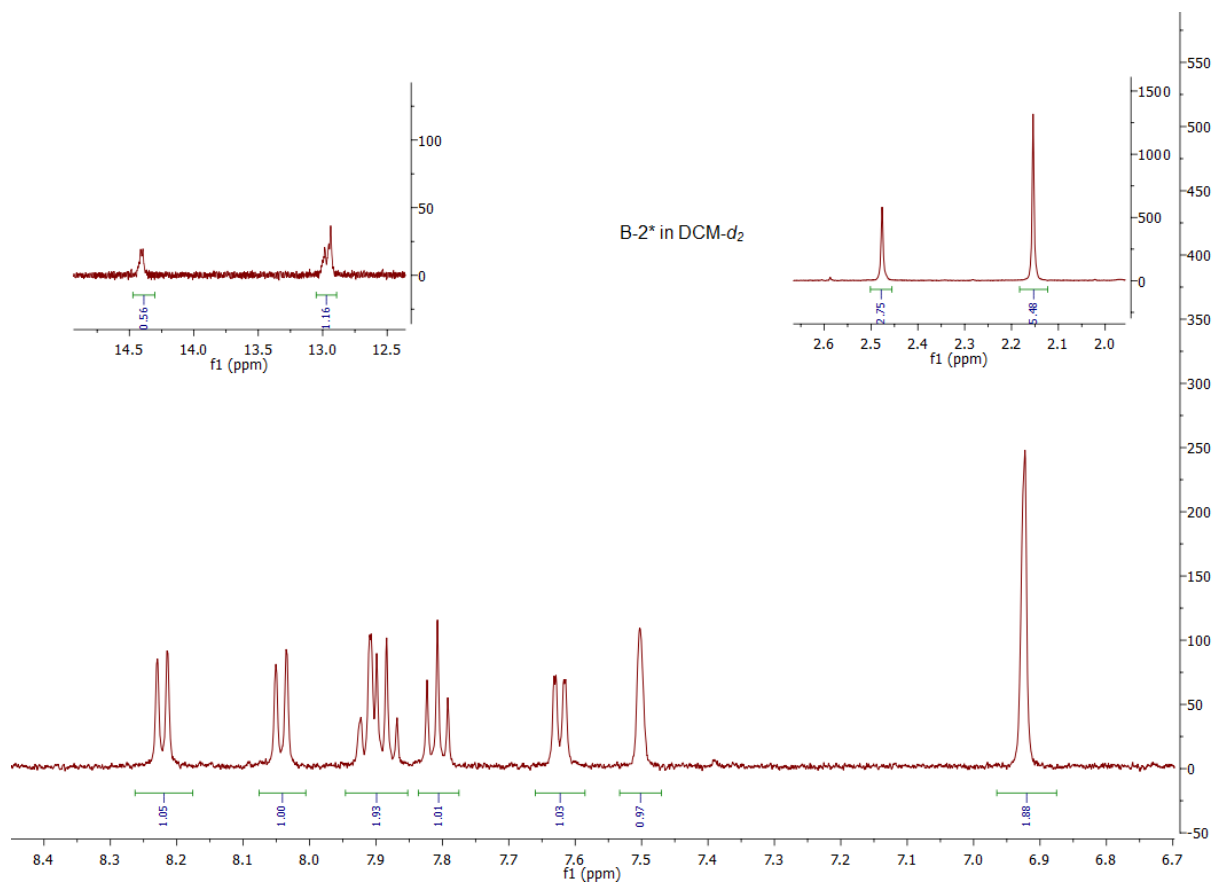


Figure S6.  $^1\text{H}$  NMR of **B-2\*** in in dichloromethane- $d_2$  (DCM- $d_2$ ).

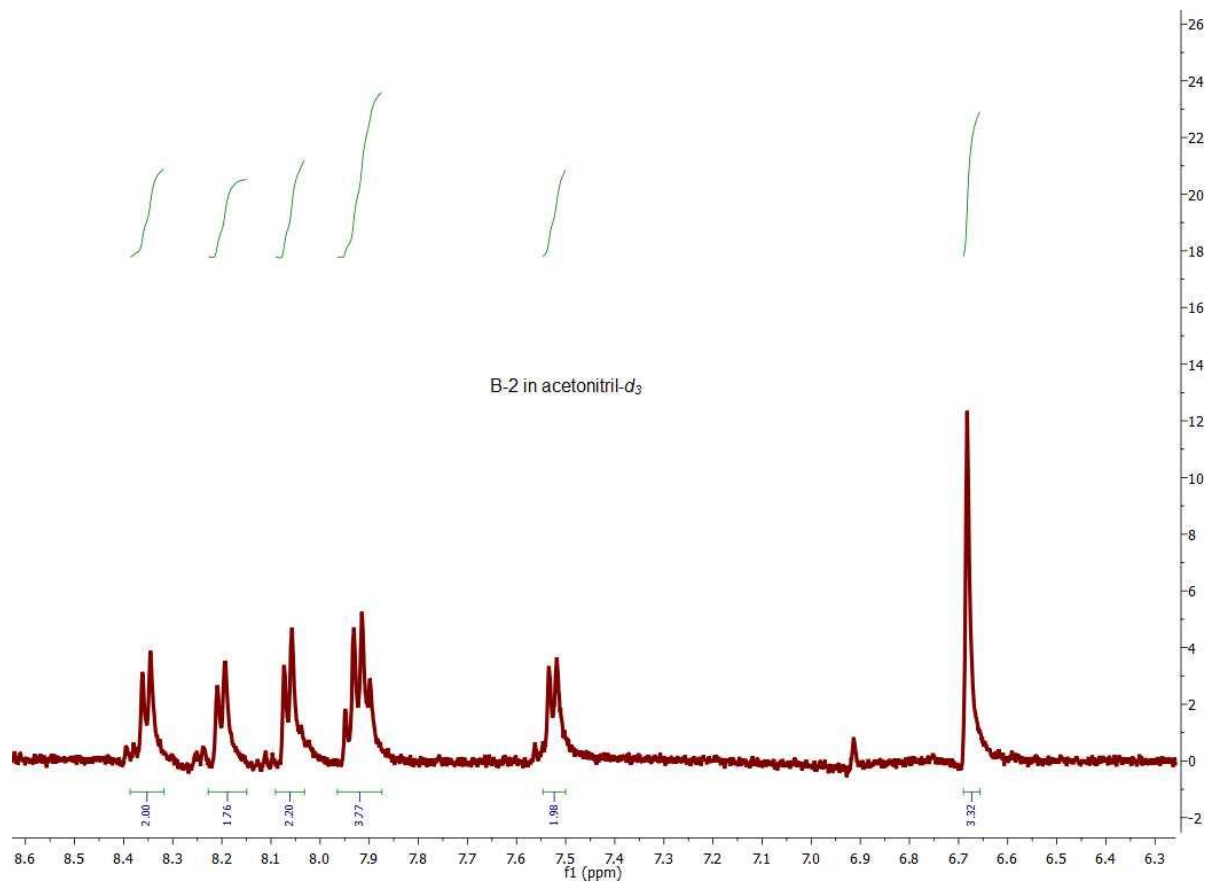


Figure S7.  $^1\text{H}$  NMR of B-2 in in acetonitril- $d_3$ . (methyl group of 4-bromo, 3-methyl pyrazole is merged with the solvent peak and are therefore not shown)



## O<sub>2</sub> DETECTION

Ce<sup>IV</sup> in pH 1.0 solutions for kinetic and stoichiometric measurements were prepared from (NH<sub>4</sub>)<sub>2</sub>Ce(NO<sub>3</sub>)<sub>6</sub> (99.99+%, Aldrich) and nitric acid (trace metal grade, 70%, purified by re-distillation, 99.999%, Fisher Scientific). The oxygen evolution data was monitored by a pressure transducer (Omega PX138-030A5 V) driven by a power supply (TTi-PL601) at 8.00 V versus time, then the amount of oxygen was calibrated by GC (GC-2014 Shimadzu). First, the solution of (NH<sub>4</sub>)<sub>2</sub>[Ce(NO<sub>3</sub>)<sub>6</sub>] in 0.1 M HNO<sub>3</sub> (3.2 mL) was added into the flask, then the aqueous solution of the catalyst (20–400 μL, 1 to 2 mM) containing 20% in volume of TFE were injected into the above solution under vigorous stirring at ambient temperature (20 °C). Secondly, 500 μL gas phase of the air tight flask was analyzed by Gas chromatography (GC). The end-point oxygen generated was converted to TON as reported (the oxygen in air present in the flask prior measurement was subtracted from the final value).

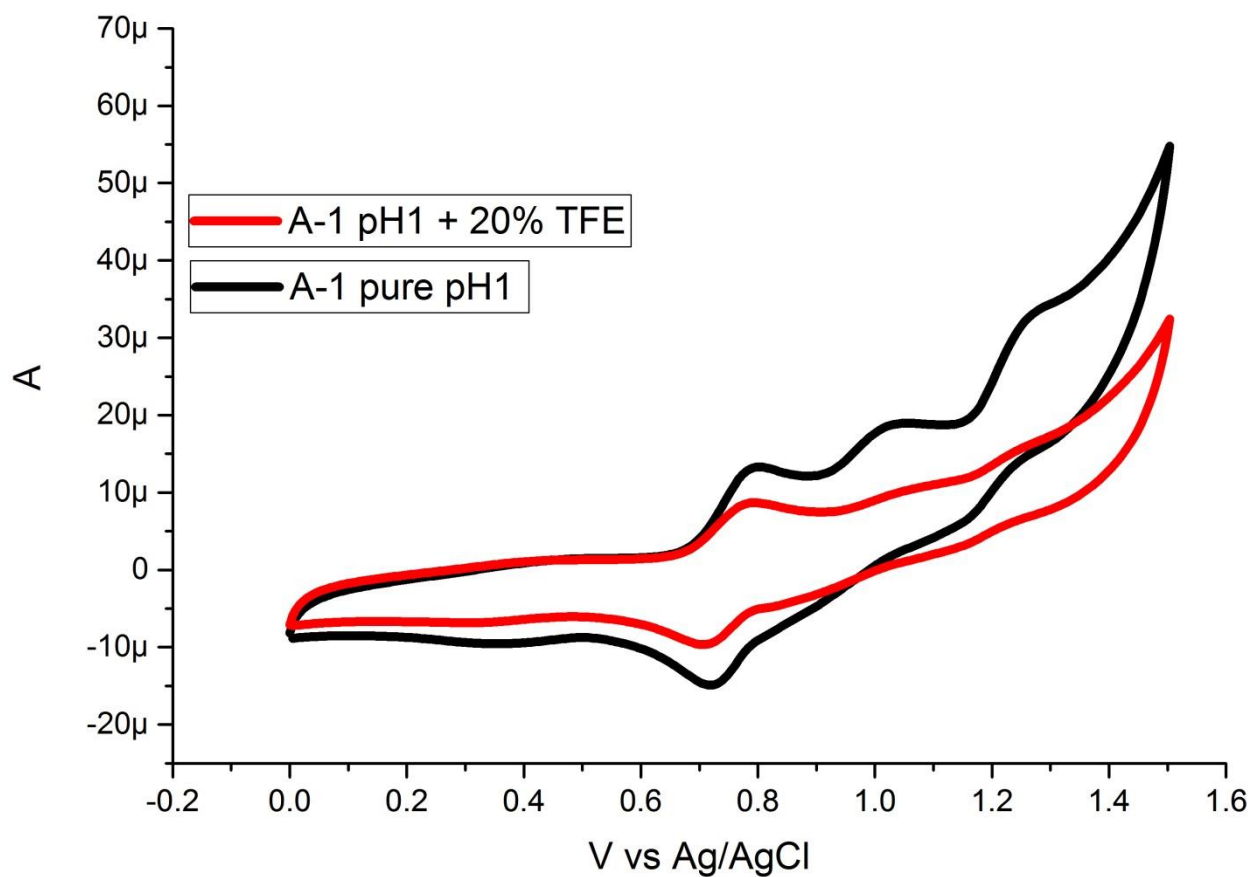


Figure S8. CVs of the influence of the 2,2,2-Trifluoroethanol (TFE) on the activity and the peak definition. Condition: 1mM catalyst, scan rate 100mV/s, Ionic Strength: 0.1.

## DIFFERENTIAL PULSE VOLTAMMETRY

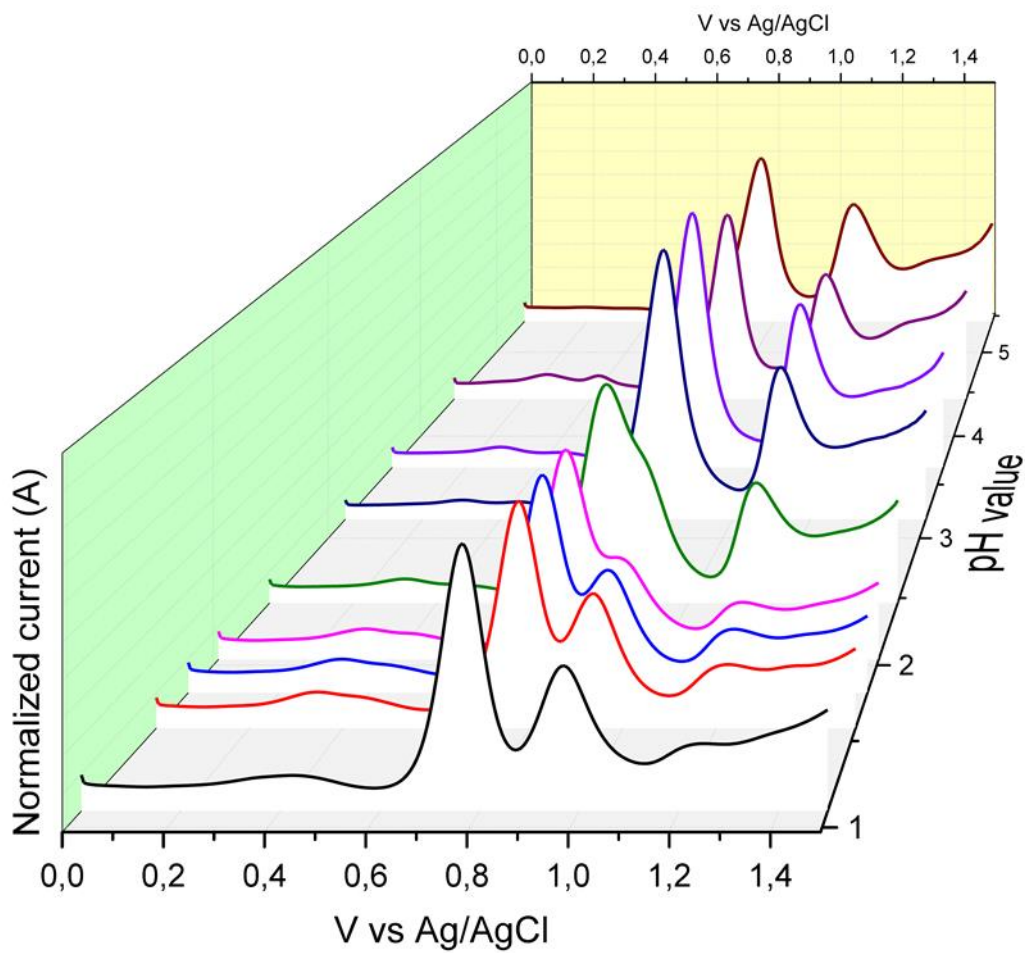


Figure S9: DPV scans at various pH of A-1 for the realisation of the Pourbaix diagram (Only few scans are shown for sake of clarity).

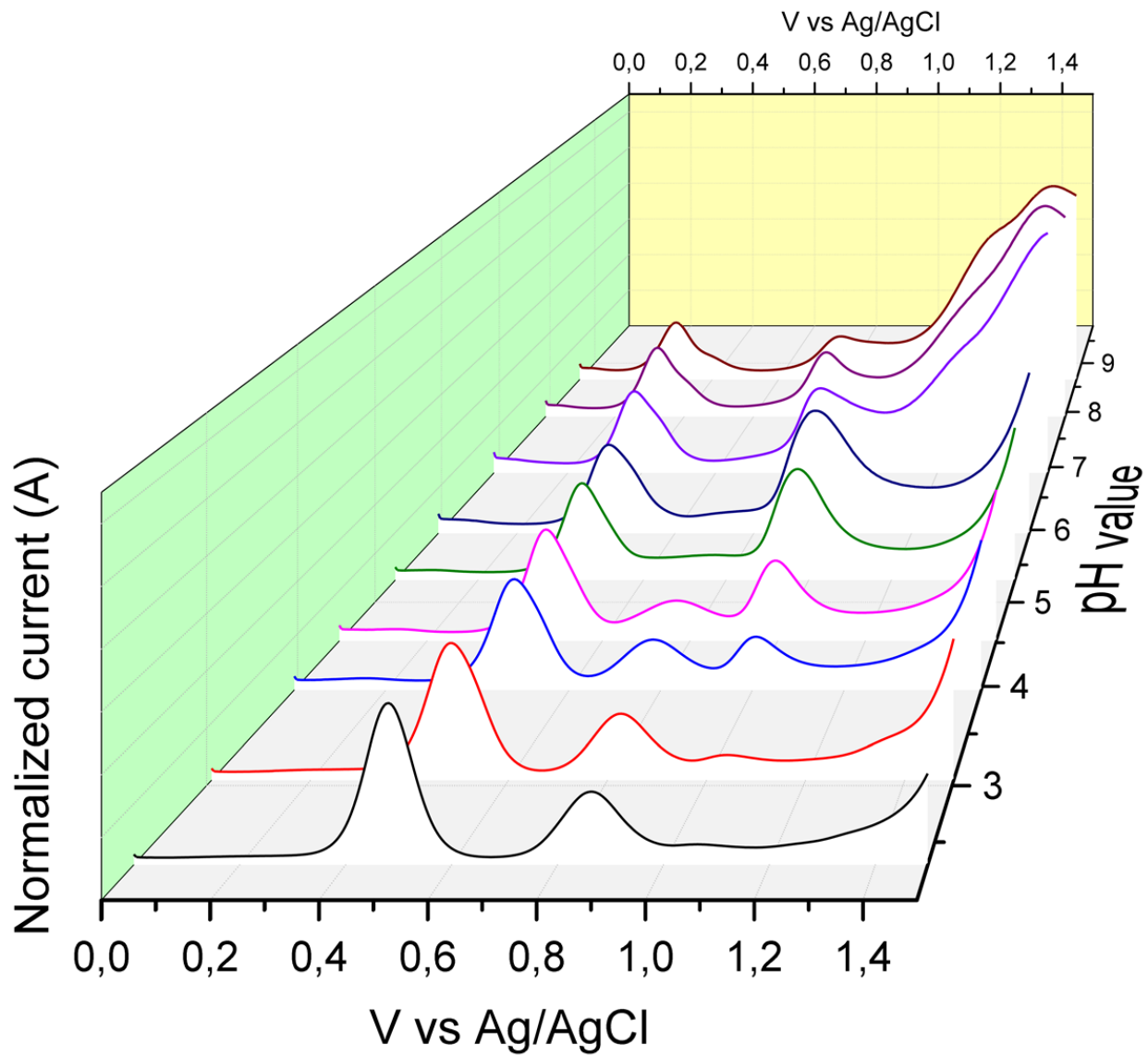


Figure S10: DPV scans at various pH of A-2 for the realisation of the Pourbaix diagram (Only few scans are shown for sake of clarity).

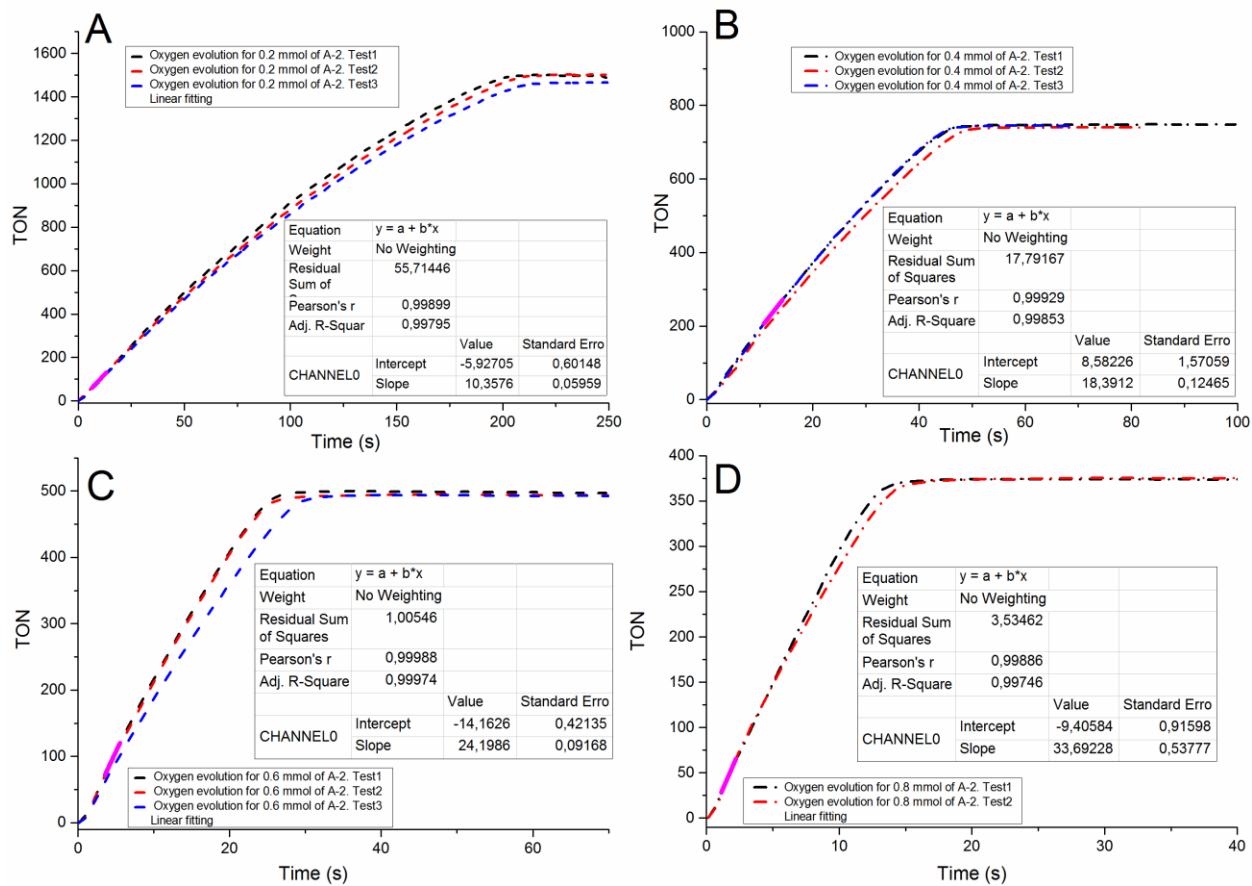


Figure S11. O<sub>2</sub> generation with different amount of A-2 under excess of Ce<sup>IV</sup> in 0.1 M HNO<sub>3</sub> solution. A) 0.2mmol of A-2; B) 0.4mmol of A-2; C)0.6mmol of A-2; D)0.8mmol of A-2.

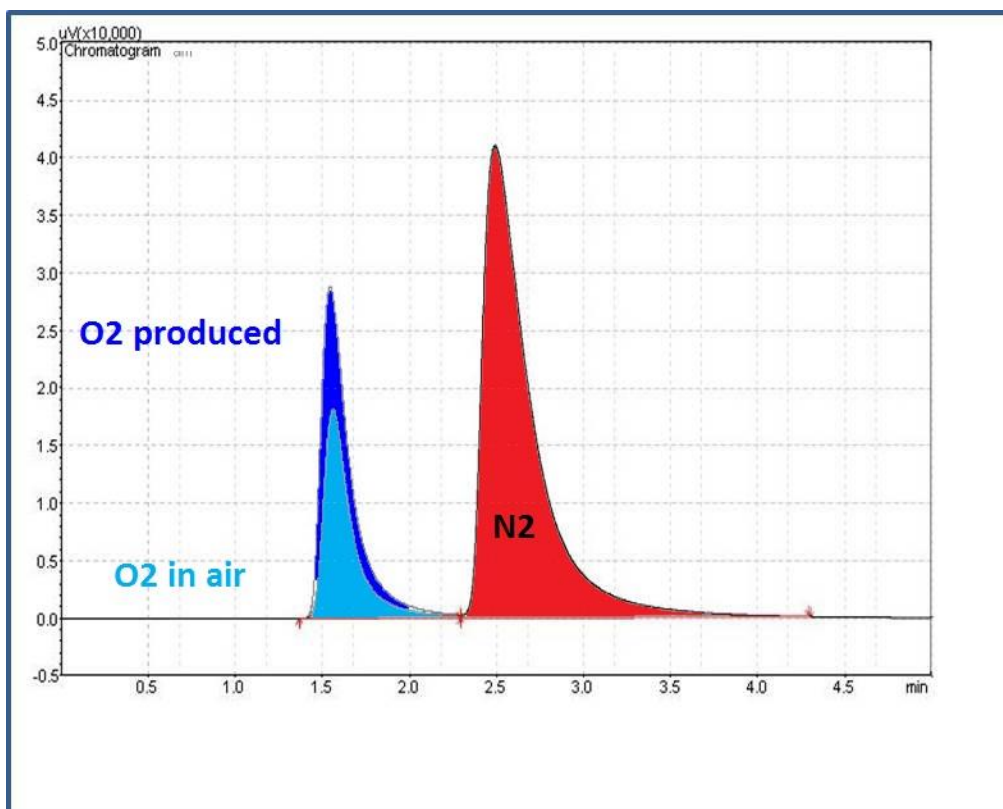


Figure S12. Detection of the oxygen produced by **A-2** under  $\text{Ce}^{\text{IV}}$  conditions by gas chromatography (GC).